

Classifying Histopathologic Glioblastoma Sub-regions with EfficientNet

Sanyukta Adap¹, Ujjwal Baid^{1,2,3,*}, and Spyridon Bakas^{1,2,3,4,5,6,*}

¹ Division of Computational Pathology, Department of Pathology & Laboratory Medicine, Indiana University School of Medicine, Indianapolis, IN, USA

² Indiana University Melvin and Bren Simon Comprehensive Cancer Center, Indianapolis, IN, USA

³ Department of Radiology & Imaging Sciences, Indiana University School of Medicine, Indianapolis, IN, USA

⁴ Department of Biostatistics & Health Data Science, Indiana University School of Medicine, Indianapolis, IN, USA

⁵ Department of Neurological Surgery, Indiana University School of Medicine, Indianapolis, IN, USA

⁶ Department of Computer Science, Luddy School of Informatics, Computing, and Engineering, Indiana University, Indianapolis, IN, USA

* Equal senior corresponding authors: ubaid@iu.edu, spbakas@iu.edu

Abstract. Glioblastoma (GBM) is the most common aggressive fast-growing brain tumor, with a grim prognosis. Despite clinical diagnostic advancements, there have not been any substantial improvements to patient prognosis. Histopathological assessment of excised tumors is the first line of clinical diagnostic routine. We hypothesize that automated, robust, and accurate identification of distinct histological sub-regions within GBM could contribute to morphologically understanding this disease at scale. In this study, we designed a four-step deep learning approach to classify such histopathological regions and quantitatively evaluated it on the BraTS-Path 2024 challenge dataset, which includes Hematoxylin & Eosin (H&E) stained GBM tissue sections annotated for six distinct regions. We used the challenge's publicly available training dataset to develop and evaluate the effectiveness of several variants of EfficientNet architectures (i.e., B0, B1, B2, B3, B4). EfficientNet-B1 and EfficientNet-B4 achieved the best performance, achieving an F1 score of 0.980 in a 5-fold cross-validation configuration using the BraTS-Path training set. We further evaluated the performance of our proposed approach on the BraTS-Path hold-out validation data and achieved F1 scores of 0.546 and 0.438 for EfficientNet-B1 and EfficientNet-B4, respectively. The difference in the performance on training and validation data highlights the challenge of developing models that generalize well to new data, which is crucial for clinical applications.

Keywords: Glioblastoma · Classification · EfficientNet · Ensemble models.

1 Introduction

Glioblastoma (GBM) are a fast-growing brain tumor affecting the functional brain tissue and its surroundings. Prognostically, the median survival of GBM patients is about 12-18 months post diagnosis and following standard-of-care treatment, however, early diagnosis can significantly impact the patient survival outcomes [3]. A significant proportion of GBM have an unknown cause. Some risk factors include previously undergone radiation therapy and hereditary conditions like neurofibromatosis and Li-Fraumeni syndrome. Typically, diagnosis is made using MRI or CT scans, followed by the histopathological assessment of a tissue biopsy [7]. GBMs have a diverse genetic

profile with heterogeneous microenvironmental histopathologic characteristics and a highly infiltrative nature. Accurately identifying these tumors and evaluating their heterogeneity is crucial for determining the best course of action and potentially improving patient survival rates [4].

Whole Slide Imaging (WSI) has become increasingly important in addressing this challenge of accurately detecting tumors, assessing their diverse histopathological features, and offering deeper insights into the tumor microenvironment. WSIs are digitized tissue sections, enabling the detailed examination of distinct morpho-pathological characteristics across large, high-resolution images. This technology paired with artificial intelligence (AI) analysis can contribute to furthering our understanding of this disease and provide information for more accurately diagnosing GBM, and hence guiding appropriate treatment strategies. Some of the key distinct histologic sub-regions in GBM tissue sections that can be identified through WSIs include [4]:

1. Cellular Tumor (CT): A region characterized by high tumor cell density.
2. Geographic Necrosis (NC): Indicative of rapid tumor growth and poor prognosis.
3. Infiltration into the Cortex (IC): Tumor invasion into cortical regions.
4. Pseudopalisading Necrosis (PN): Areas where tumor cells surround and line up around necrotic tissue.
5. Microvascular Proliferation (MP): The formation of abnormal, new blood vessels within a tumor.
6. Penetration into White Matter (WM): The invasion and spread of tumor cells into the brain's white matter tissue.

With recent advancements in AI and data availability, it has become easier to train AI models to automate the identification and classification of GBM [17–19]. Furthermore, we note a proliferation of open-source publicly available data registries that include large, multi-institutional databases of clinical, imaging, and molecular datasets of GBM [9–13, 20, 21, 4]. Some of the most popular ones are TCGA-GBM [10], Ivy GAP [11], BraTS-Path [4], UPenn-GBM [20], UCSF-PDGM [21], ReSPOND [23], NCBI-GEO [12], NCBI-dbGaP [13], and iGLASS [24].

This study proposes a four-step deep learning approach (Figure 1) for classifying histopathological regions in GBM using the EfficientNet architecture. The presented method was designed and submitted for evaluation as part of the Brain Tumor Segmentation - Pathology (BraTS-Path) Challenge. The main goal of the BraTS-Path challenge is to generate a publicly available dataset and a benchmark platform for deep-learning models that can classify patches of digitized histopathology tissue sections of GBM. The images in the dataset are classified into 6 regions of interest, i.e., CT, PN, MP, NC, IC, and WM [4]. We evaluated different EfficientNet variants on the BraTS-Path dataset to assess their ability to classify these clinically-relevant GBM tissue regions. By addressing model complexity and overfitting, EfficientNet aims to create a reliable model for more precise diagnosis and personalized treatment planning for GBM patients.

2 Materials and Methods

2.1 Data

The BraTS-Path challenge was hosted on the Synapse Platform [22]. The participants were provided datasets in 2 phases: training and validation. The labels were provided for the training data but not for the validation data. During the validation phase, the participants were asked to submit their predictions on validation data in a CSV file on the Synapse evaluation platform. Finally, during

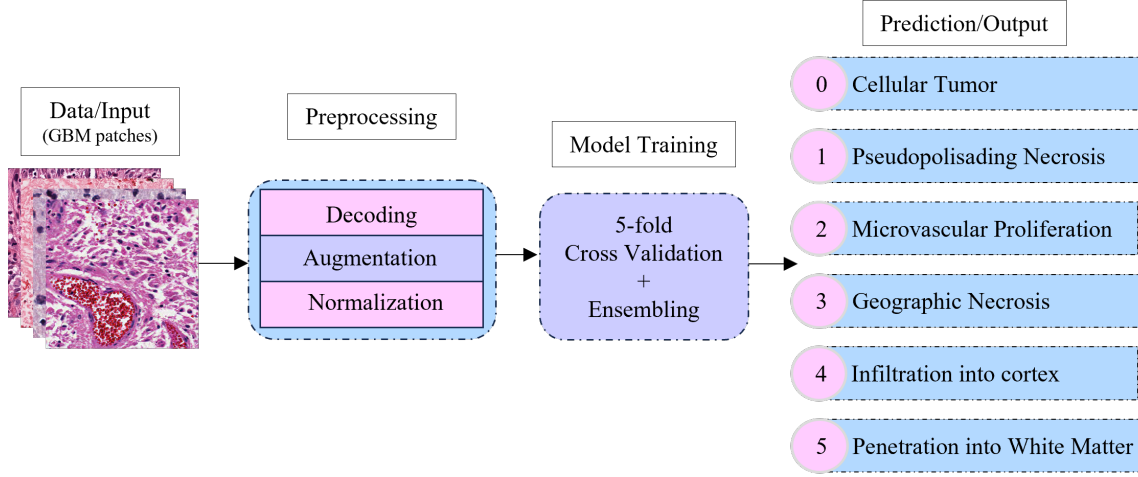


Fig. 1. Overview of our proposed methodology. The BraTS-Path dataset (GBM patches) undergoes a set of pre-processing steps to make the images compatible with model training. We feed the images in mini-batches to the model for training in a 5-fold cross-validation manner. During inference, we ensemble the best model from each fold and output the prediction based on the average output from all folds, combined.

the testing phase, participants were asked to submit an MLCube container image of their model inference pipeline for evaluation on the hidden test dataset.

The training dataset consisted of 96,485 images divided into 6 distinct histological regions. The images were in PNG format and 512x512 pixels with 3 channels (RGB). The pixel values ranged from 0 to 255. The data distribution for each class can be found in Table 1, along with some sample representative images of each class in Figure 2. The challenge validation dataset consisted of 36,401 images of the same size and shape whose labels were not provided to the participants.

We divided the challenge’s training dataset into our internal training and validation cohorts using an 80:20 split, each of them proportional to the given classes.

2.2 Pre-processing

Ensuring the input data is clean, consistent, and representative of the task, allows the CNN to learn efficiently and generalize effectively to new data. This crucial step is fundamental for achieving

Table 1. BraTS-Path Training Set Distribution.

Class	Count	%
Cellular Tumor (CT)	34139	35%
Geographic Necros (NC)	29542	31%
Infiltration into Cortex (IC)	14500	15%
Pseudopolisading Necrosis (PN)	9664	10%
Microvascular Proliferation (MP)	4812	5%
Penetration into White Matter (WM)	3828	4%
Total	96,485	100%

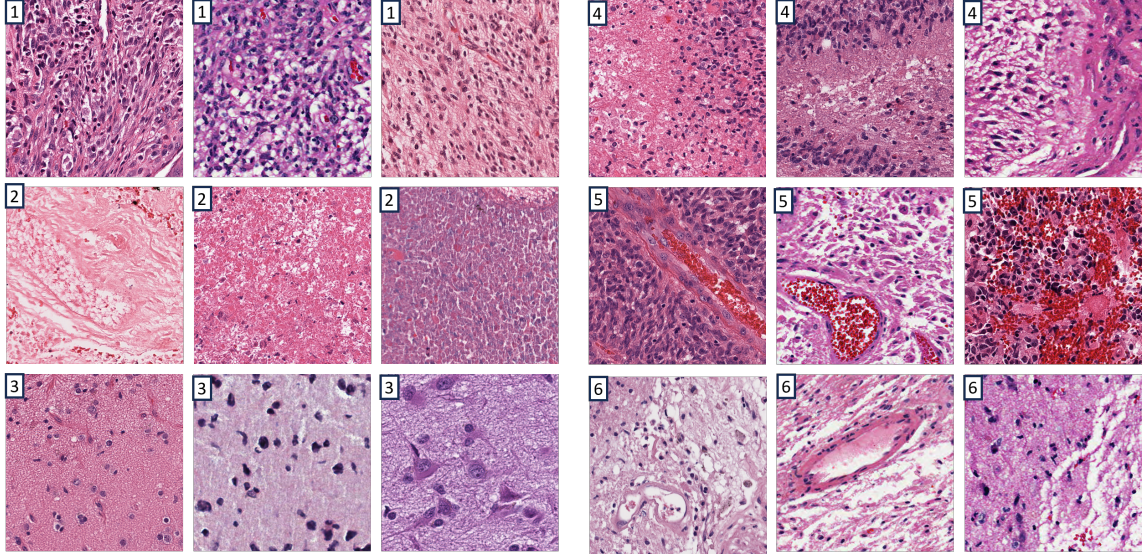


Fig. 2. Sample images in the training data. 1-Cellular Tumor (CT), 2-Pseudopalisading Necrosis (PN), 3-Infiltration into Cortex (IC), 4-Geographic Necrosis (NC), 5-Microvascular Proliferation (MP), and 6-Penetration into White Matter (WM).

precise and dependable outcomes in any CNN-based application. For this, we pre-processed data in three steps: 1) Decoding, 2) Data Augmentation, and 3) Normalization, towards ensuring smooth and efficient training.

Decoding: Decoding is a process of converting input images to PyTorch tensors. The images were transformed into numerical arrays that represented the pixel values from the original PNG image. To make the pixel intensities appropriate for AI methods, they must be converted into multi-dimensional arrays or tensors. For gray-scale images, every pixel value within these arrays represents its intensity; for color images, it represents its RGB components.

Data Augmentation: During this pre-processing stage, images are augmented to enhance the dataset's variability by implementing a series of transformations. These include random rotations up to 20 degrees, random horizontal and vertical flips, as well as random modifications to brightness and contrast by 0.1. These augmentations generate diversity by creating different variations of each image, thus increasing the number of unique data points with every iteration through the dataset.

Normalization: Further, the pixel values of each image were normalized to a floating-point type and scaled to the range [0, 1]. The scaling was done by first calculating the mean and standard deviation for all the images in the mini-batch. Then, the images were normalized using (1):

$$Z_i = \frac{X_i - \mu}{\sigma + \epsilon} \quad (1)$$

Where, μ is the global mean of the image set X , σ is the standard deviation, $\epsilon = 1 \times 10^{-10}$ is a very small constant added to the denominator which prevents the denominator from turning zero, $i = [1 - 2083]$ is the index of each training sample, and Z_i is the normalized version of X_i . Normalization ensures that the inputs in the batch are on a similar scale. Normalizing/standardizing inputs has several benefits:

1. It prevents a particular feature with a higher pixel value from dominating the others in the learning process.
2. The gradients that direct the model learning are more balanced, which lowers the likelihood of oscillations or slow convergence during training.
3. It also minimizes the instability caused by the larger numerical values, leading to more consistent results across different batches.
4. By standardizing the scale of input images, the model, instead of learning specific pixel value ranges, can better understand the underlying patterns in the data.

2.3 Model Training

EfficientNet: EfficientNets [6] (ENets) are a range of models that have made model scaling more systematic by balancing the depth (number of layers), width (number of channels), and input image resolution of CNN models using predefined scaling coefficients. This approach is referred in the literature as compound scaling, and the coefficients for depth (d), width (w), and resolution (r) are defined as:

$$d = \alpha^\phi \quad (2)$$

$$w = \beta^\phi \quad (3)$$

$$r = \gamma^\phi \quad (4)$$

where α , β , γ are constants determined through grid search, and ϕ is a user-defined compound coefficient that regulates the number of additional resources that can be used for model scaling.

ENet model ranges from B0 to B7. The ENet-B0 is the smallest in the range and is considered a baseline model due to its mobile-sized architecture. The variants B1 to B7 are scaled-up versions of B0 (using different values of ϕ) systematically using (2), (3), and (4), with comparatively higher accuracy, but fewer parameters and FLOPS than existing CNNs. The ENet models have achieved state-of-the-art performance on ImageNet [8] and other well-known transfer learning datasets in 2019 and 2020 that are widely used for training and evaluation of Convolutional Neural Networks (CNNs).

In this study, we used transfer learning to train ENet-B0, ENet-B1, ENet-B2, ENet-B3, and ENet-B4 pre-trained on ImageNet [8] to train them on the BraTS-Path training data.

Cross-Validation: Cross-validation is a technique that is used to evaluate the performance of models on new unseen data. For this, the dataset is divided into equal parts. All, except one part, is used for training, whereas the one that was left out, is used as a validation set. Thus, for example, in a 5-fold cross-validation setup, we divide the dataset into 5 parts/folds. For each fold, we take 4 parts as a training set, and 1 part as the validation set. With this, we now have 5 models, each of which is validated on unique validation sets (one part of the five). Then, the combined decision of all 5 models, would be the final decision on the test set.

Loss: After one epoch of training, the model predicts the output in the form of logits for each image in the mini-batch. These outputs were passed to a Weighted Cross Entropy Loss Function, L, (5) to compute the classification error across each mini-batch.

$$L = -\frac{1}{N} \sum_{i=1}^N w_{y_i} \cdot \log(\hat{y}_i, y_i) \quad (5)$$

Where: N is the number of samples, w_{y_i} is the weight for the true class y_i of the i -th sample, \hat{y}_i is the predicted probability for the true class y_i of the i -th sample.

Metrics: After each epoch, both, training and validation (training and validation split from the original training data) metrics were calculated. We evaluated the models based on Loss (5), and F1 (8) scores per epoch. We also plotted a confusion matrix for each epoch and saved the model weights in the form of checkpoints.

$$\text{Precision} = \frac{\text{TP}}{\text{TP} + \text{FP}} \quad (6)$$

$$\text{Recall} = \frac{\text{TP}}{\text{TP} + \text{FN}} \quad (7)$$

$$\text{F1} = 2 \cdot \frac{\text{Precision} \cdot \text{Recall}}{\text{Precision} + \text{Recall}} \quad (8)$$

2.4 Inference

For inference, the final set of hyperparameters, shown in Table 2, was used to train the top-performing models in a 5-fold cross-validation manner. We selected 5 models, one from each fold, and ensembled their logits by taking their average and then applying a softmax function over it. This way, we combine the results from each “weak” model to form one “strong” model, that can classify the images much better and robust than each of the individual models, and while avoiding systematic biases of the individual models.

2.5 Experimental Design

We conducted all experiments on Indiana University’s High-Performance Computing Cluster, BigRed200, which has 256 GB of memory, a single 64-core, 2.0 GHz, 225-watt AMD EPYC 7713 processor, and four NVIDIA A100 GPUs. The codebase of this study is exclusively built on Python/PyTorch [5].

We have referred to the validation data provided by the challenge as “Challenge Validation Data” since the labels were not provided to the participants. All models were initially evaluated on our internal validation split (created from the labeled BraTS-Path training dataset provided by the challenge organizers), and the final quantitative performance evaluation of our proposed approach was conducted on the challenge validation data. We carried out the following experiments to identify the optimal model.

First, the models were trained without cross-validation to identify which ENet models performed better on the challenge validation data provided by the challenge. We also experimented with

Table 2. Experiment Hyperparameters.

Hyperparameters	Value
Batch Size	16
Number of Epochs	60
Loss Function	Cross Entropy Loss
Optimizer	Adam
Momentum	0.0001
LR	0.001
LRS	Exponential
Gamma	0.9

Learning Rate Schedulers (LRS)[14] along with different rates of LR Decay (gamma). LRS is a method that tweaks the LR by a factor during training. This allows for a staged fine-tuning of the LR by enabling the model to make larger updates early in the training process when the parameters are far from optimal and smaller updates later on when the parameters are closer to the minima. For the experiments, we used 3 LRS provided by PyTorch:

1. Step LR: This decays the LR by a factor of gamma at every predetermined period of LR decay.
2. Multi-step LR: This decays the LR by a factor of gamma at a predefined epoch number.
3. Exponential LR: This decays the learning rate by a factor of gamma at every epoch.

All the models were trained for 60 epochs. For optimization, we used Adam [14] with a momentum of 0.0001. We performed multiple rounds of training in combination with different hyperparameters to find the models that had the best performance on the internal validation split.

Then, with the top 2 models that performed best on the challenge validation data, we trained the models in a 5-fold cross-validation manner with the best combination of hyperparameters. For each fold, the input images, after pre-processing, were passed to the models in mini-batches of size 16. The model performs feature extraction, followed by batch normalization, and adaptive average pooling. Finally, the images were passed to the classification layer of size 6 (number of classes).

Once all models had their respective predictions, we combined their results by averaging the outputs from each fold. This averaged output, is the final prediction which was submitted for evaluation on the challenge validation data.

3 Results

3.1 Model Training

The initial training without cross-validation revealed that ENet-B1 and ENet-B4 were the top 2 models among the 5 with a challenge validation F1 of 0.462 and 0.43, respectively. Table 3 presents the results from the initial experiments on the ENet Models (using hyperparameters mentioned in Table 2) along with their performance metrics on the challenge validation dataset.

Further experiments with LRS show that exponential LRS with a gamma of 0.9 yielded the best performance on the internal validation split. See Figure 3 for training curves.

Next, with the final set of hyperparameters, we trained ENet-B1 and ENet-B4 in a 5-fold cross-validation manner. The performance of both the models across all folds during the complete training was almost identical (Figure 4). Specifically, the convergence curves relative to both the performance evaluation metric (F1) and loss are overlapping.

Table 3. Initial Training Experiments

Model	Challenge Validation F1	Challenge Validation MCC
ENet-B0	0.288	0.242
ENet-B1	0.462	0.374
ENet-B2	0.345	0.262
ENet-B3	0.274	0.214
ENet-B4	0.43	0.336

3.2 Inference

Once the models were trained, we chose model checkpoints across all folds at epochs 20, 25, 30, and 35. Then, for each ENet model, we chose a model checkpoint for each fold, and combined/ensembled their predictions on the challenge validation data. The results of both models with model checkpoints at different epochs are shown in Table 4.

4 Discussion

In this study we presented a 4-step deep learning approach with an EfficientNet model that can robustly classify 6 histologic distinct GBM regions. We mainly focused on training ENet models with the BraTS-Path training data and evaluated them using the BraTS-Path validation data. According to the results obtained from various experiments, the performance metrics of ENet-B1 seem to be higher than those of ENet-B4. This could be due to the larger and more complex architecture of ENet-B4 compared to ENet-B1.

Beyond Enets, during the initial screening of models, along with ENet variants, we also evaluated the ResNet [15] and DenseNet [16] variants. However, these models demonstrated significantly lower performance compared to the ENet models that led to the decision of excluding their results from this manuscript. The disparity in performance can be explained by several key factors. While ResNet and DenseNet architectures are undeniably powerful, they lack the level of architectural efficiency and optimization found in ENet. ENet’s compound scaling approach allows it to achieve higher performance with fewer parameters. Moreover, ENet leverages advanced design techniques like Mobile Inverted Bottleneck Convolutions (MBConv) and depthwise separable convolutions, which are both computationally efficient and improve the model’s generalization capabilities. In contrast, the lower performance of ResNet and DenseNet in our evaluations can likely be attributed to their

Table 4. Challenge Validation Set Metrics by Ensembling the predictions across folds.

Model	Model Checkpoint	Challenge Validation F1	Challenge Validation MCC
ENet-B1	25	0.491	0.388
ENet-B1	30	0.546	0.436
ENet-B1	35	0.53	0.421
ENet-B4	20	0.403	0.311
ENet-B4	25	0.438	0.337
ENet-B4	30	0.39	0.301

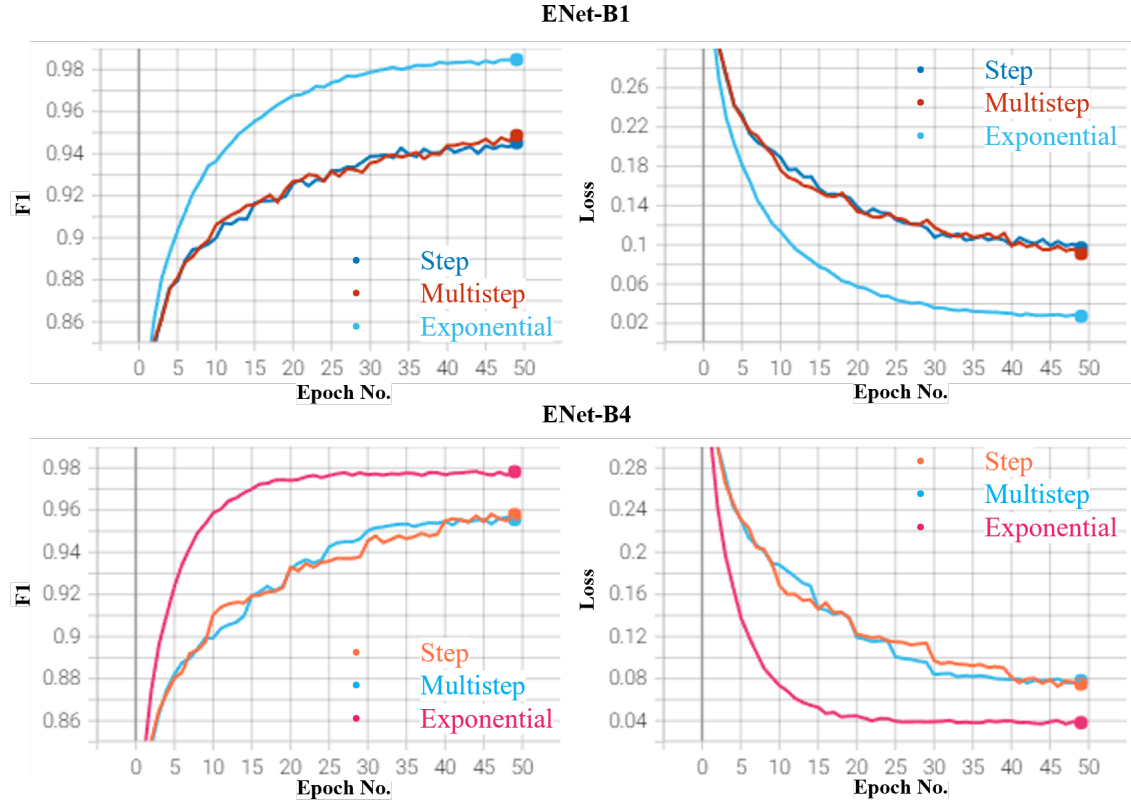


Fig. 3. Training F1 scores and Loss Curves for ENet-B1 and ENet-B4 per Epoch with Gamma = 0.9.

less optimized use of computational resources and parameters, despite their complex and deep designs. As a result, their outcomes did not warrant inclusion in the final analysis.

Further experimentation with LRS revealed that exponential LRS with gamma equal to 0.9 had the best performance. This could be likely due to a smooth and gradual decaying of LR over the epochs. Since exponential LRS reduces LR exponentially over the epochs, we used an LR of 0.001, which is a slightly higher value if used without LRSs. However, an exponential LRS ensured that the LR remained sufficiently high during the early epochs to learn quickly and gradually reduced it as the model approached better parameter estimates, leading to improved validation performance over time.

The small difference between the training and validation metrics can be attributed to the fact that the validation set was derived from the same dataset obtained from the challenge training website. This dataset was split into 80% for training and 20% for validation, meaning the validation set was “in-sample” and not truly independent. As a result, the model’s performance on this validation set was high (0.95+). In contrast, the challenge validation set likely had a different, “out-of-sample” distribution, leading to lower scores when evaluated on that cohort.

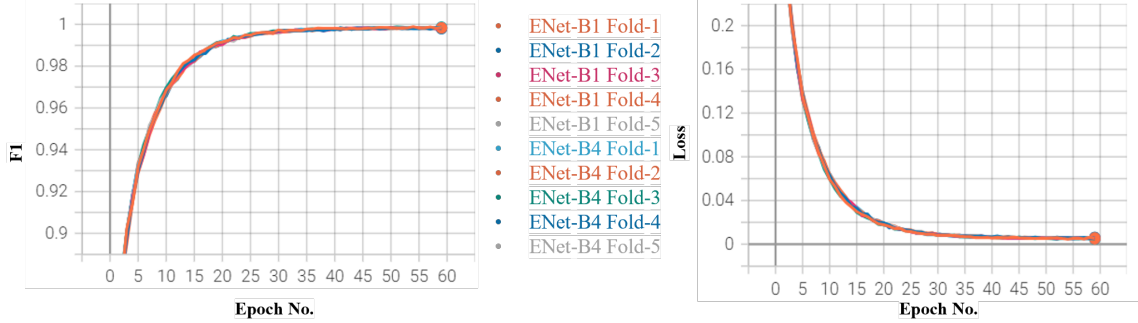


Fig. 4. Cross Validation Training Metric Curves for ENet-B1 and ENet-B4 per Epoch.

Overall, ENet-B1 and ENet-B4 training both followed a fairly similar trend. The models' performance on the training set was comparable, reflected by the overlapping training loss and F1 curves shown in Figure 4, suggesting that both models could learn from the training data effectively and without fluctuations throughout the training process. Furthermore, it implies that both models are proficient in identifying the fundamental characteristics of the training data from BraTS-Path. The simpler ENet-B1 generalizes better to challenge data than the more complicated ENet-B4, but the difference in performance on the challenge validation data emphasizes the significance of model complexity and the possibility of overfitting. This result highlights how important it is to maintain a balance in machine learning tasks between model complexity and its ability to generalize the data.

The implications of our study are significant for the field of computational pathology and the diagnosis of GBM. It suggests that simpler models like ENet-B1 may generalize better to new data, when compared to more complex models, which can overfit despite their larger capacity. This highlights the need to balance model complexity with generalization, especially in medical applications where accuracy is crucial. Additionally, the study underscores the importance of diverse training datasets to improve performance on real-world cases, potentially leading to more reliable AI-driven diagnostic tools and better patient outcomes.

Our contribution demonstrates that a streamlined model like ENet-B1 can achieve superior generalization in GBM classification compared to more complex architectures. This challenges the conventional focus on larger models and suggests that efficiency and simplicity may often lead to better performance in certain medical contexts. Additionally, our study underscores the importance of dataset diversity in developing models that can be trusted in real-world clinical applications.

The study advances our understanding of GBM classification by demonstrating that simpler models like ENet-B1 can generalize effectively to unseen data, a crucial factor in accurately diagnosing brain tumors. It reveals that complex models, prone to overfitting, may not always be ideal for biological data where variability is high. This insight highlights that efficiency and simplicity in model architecture can enhance performance in medical applications by better capturing the essential biological features of GBM. Furthermore, the research emphasizes the necessity of diverse and representative training datasets to reflect the biological diversity of real-world cases, ultimately improving the robustness and clinical applicability of AI-driven diagnostic tools.

Despite the results, there are several limitations in this study. Firstly, the BraTS-Path training dataset may not accurately reflect the diversity of GBM cases seen in clinical settings. Furthermore, the BraTS-Path multi-institutional training data was split into training and validation cohorts, po-

tentially resulting in an “in-sample” situation that would have inflated the validation performance metrics. Since the challenge validation set and the labeled validation split appear to come from completely different distributions, this setup does not mirror real-world conditions where the validation set should ideally represent the test data. In practice, the validation set serves as a proxy for unseen test data, and it should reflect the characteristics of that test data to provide a meaningful estimate of how the model will generalize. If the validation set is too similar to the training set, it may lead to inflated performance estimates and failure to accurately assess model robustness. Moreover, we did not investigate the effects of regularization methods such as data augmentation, which may reduce overfitting in larger models. Lastly, we focused on one particular model, the ENet, without exploring other architectures that might offer a better trade-off between generalization and complexity. While several state-of-the-art models may have been better suited for this task, the strict timeline of the challenge and our limited computational resources necessitated the exclusive use of ENet models. This choice allowed us to strike a balance between performance and efficiency, helping us meet the challenge’s deadlines while making the most of the resources available.

Future directions might focus on mitigating these limitations by extending the dataset to encompass more diverse sources of data, thereby better representing the heterogeneity of GBM cases observed in clinical settings. Furthermore, the reliability of model evaluation may be increased by using cross-validation procedures but with carefully chosen validation sets that more closely resemble the real-world test data. Additionally, experimenting with various current state-of-the-art architectures, using regularization strategies (data augmentation and dropout), and utilizing a different optimizer may improve the robustness and generalization of the model. Future research may be able to solve these issues to provide more promising outcomes.

With this study, we aimed to develop a deep learning model that can accurately classify histopathological regions in GBM tissue sections, with the ultimate objective of improving diagnostic accuracy and facilitating quantitative studies towards furthering our disease understanding. By leveraging the ENet architecture and utilizing the BraTS-Path challenge dataset [4], our goal was to create a robust and generalizable model capable of distinguishing critical histopathological features of GBM. This approach is intended to aid clinicians in making more informed decisions, potentially leading to better patient outcomes and more effective management of this aggressive and rare form of brain cancer.

Acknowledgments

This research was supported in part by Lilly Endowment, Inc., through its support for the Indiana University Pervasive Technology Institute.

References

- Yalamarty, S.S.K., Filipczak, N., Li, X., Subhan, M.A., Parveen, F., Ataide, J.A., Rajmalani, B.A. and Torchilin, V.P., 2023. Mechanisms of resistance and current treatment options for glioblastoma multiforme (GBM). *Cancers*, 15(7), p.2116.
- Gallego, O., 2015. Nonsurgical treatment of recurrent glioblastoma. *Current oncology*, 22(4), pp.273-281.
- Bleeker, F.E., Molenaar, R.J. and Leenstra, S., 2012. Recent advances in the molecular understanding of glioblastoma. *Journal of neuro-oncology*, 108, pp.11-27.
- Bakas, S., Thakur, S.P., Faghani, S., Moassefi, M., Baid, U., Chung, V., Pati, S., Innani, S., Baheti, B., Albrecht, J. and Karargyris, A., 2024. BraTS-Path Challenge: Assessing Heterogeneous Histopathologic Brain Tumor Sub-regions. arXiv preprint arXiv:2405.10871.

5. Paszke, A., Gross, S., Massa, F., Lerer, A., Bradbury, J., Chanan, G., Killeen, T., Lin, Z., Gimelshein, N., Antiga, L. and Desmaison, A., 2019. Pytorch: An imperative style, high-performance deep learning library. *Advances in neural information processing systems*, 32.
6. Tan, M. and Le, Q., 2019, May. EfficientNet: Rethinking model scaling for convolutional neural networks. In *International conference on machine learning* (pp. 6105-6114). PMLR.
7. Kanderi, T., Munakomi, S. and Gupta, V., 2024. Glioblastoma multiforme. In *StatPearls* [Internet]. StatPearls Publishing.
8. Deng, J., Dong, W., Socher, R., Li, L.J., Li, K. and Fei-Fei, L., 2009, June. Imagenet: A large-scale hierarchical image database. In *2009 IEEE conference on computer vision and pattern recognition* (pp. 248-255). Ieee.
9. Yearley, A.G., Iorgulescu, J.B., Chiocca, E.A., Peruzzi, P.P., Smith, T.R., Reardon, D.A. and Mooney, M.A., 2022. The current state of glioma data registries. *Neuro-Oncology Advances*, 4(1), p.vdac099.
10. Bakas, S., Akbari, H., Sotiras, A., Bilello, M., Rozycski, M., Kirby, J.S., Freymann, J.B., Farahani, K. and Davatzikos, C., 2017. Advancing the cancer genome atlas glioma MRI collections with expert segmentation labels and radiomic features. *Scientific data*, 4(1), pp.1-13.
11. Ivy Glioblastoma Atlas Project Homepage, <https://glioblastoma.alleninstitute.org/>, last accessed 2024/08/11.
12. NCBI, GEO Homepage, <https://www.ncbi.nlm.nih.gov/geo/>, last accessed 2024/08/11.
13. NCBI, dbGaP Homepage, <https://www.ncbi.nlm.nih.gov/gap/>, last accessed 2024/08/11.
14. PyTorch Optimization Algorithms, <https://pytorch.org/docs/stable/optim.html>, last accessed 2024/08/13.
15. He, K., Zhang, X., Ren, S. and Sun, J., 2016. Deep residual learning for image recognition. In *Proceedings of the IEEE conference on computer vision and pattern recognition* (pp. 770-778).
16. Huang, G., Liu, Z., Van Der Maaten, L. and Weinberger, K.Q., 2017. Densely connected convolutional networks. In *Proceedings of the IEEE conference on computer vision and pattern recognition* (pp. 4700-4708).
17. Babaei Rikan, S., Sorayaie Azar, A., Naemi, A., Bagherzadeh Mohasefi, J., Pirnejad, H. and Wil, U.K., 2024. Survival prediction of glioblastoma patients using modern deep learning and machine learning techniques. *Scientific Reports*, 14(1), p.2371.
18. Luckett, P.H., Olufawo, M., Lamichhane, B., Park, K.Y., Dierker, D., Verastegui, G.T., Yang, P., Kim, A.H., Chheda, M.G., Snyder, A.Z. and Shimony, J.S., 2023. Predicting survival in glioblastoma with multimodal neuroimaging and machine learning. *Journal of Neuro-oncology*, 164(2), pp.309-320.
19. Zhang, W., Dang, R., Liu, H., Dai, L., Liu, H., Adegboro, A.A., Zhang, Y., Li, W., Peng, K., Hong, J. and Li, X., 2024. Machine learning-based investigation of regulated cell death for predicting prognosis and immunotherapy response in glioma patients. *Scientific Reports*, 14(1), p.4173.
20. Bakas, S., Sako, C., Akbari, H., Bilello, M., Sotiras, A., Shukla, G., Rudie, J.D., Santamaría, N.F., Kazerooni, A.F., Pati, S. and Rathore, S., 2022. The University of Pennsylvania glioblastoma (UPenn-GBM) cohort: advanced MRI, clinical, genomics, & radiomics. *Scientific data*, 9(1), p.453.
21. Calabrese, E., Villanueva-Meyer, J.E., Rudie, J.D., Rauschecker, A.M., Baid, U., Bakas, S., Cha, S., Mongan, J.T. and Hess, C.P., 2022. The University of California San Francisco preoperative diffuse glioma MRI dataset. *Radiology: Artificial Intelligence*, 4(6), p.e220058.
22. Synapse Homepage, <https://www.synapse.org/>, last accessed 2024/08/13.
23. Davatzikos, C., Barnholtz-Sloan, J.S., Bakas, S., Colen, R., Mahajan, A., Quintero, C.B., Capellades Font, J., Puig, J., Jain, R., Sloan, A.E. and Badve, C., 2020. AI-based prognostic imaging biomarkers for precision neuro-oncology: the ReSPOND consortium. *Neuro-oncology*, 22(6), pp.886-888.
24. Bakas, S., Ormond, D.R., Alfaro-Munoz, K.D., Smits, M., Cooper, L.A.D., Verhaak, R. and Poisson, L.M., 2020. iGLASS: imaging integration into the Glioma Longitudinal Analysis Consortium. *Neuro-oncology*, 22(10), pp.1545-1546.